Int. J. Cancer: **106,** 836–847 (2003)

Publication of the International Union Against Cancer

INVOLVEMENT OF p53 IN SPECIFIC ANTI-NEUROECTODERMAL TUMOR ACTIVITY OF ALOE-EMODIN

Teresa PECERE[1,5], Federica SARINELLA[1], Cristiano SALATA[1], Barbara GATTO[2], Alessandra BET[1,5], Francesca DALLA VECCHIA[3], Alberto DIASPRO[4], Modesto CARLI[5] Manlio PALUMBO[2] and Giorgio PALÙ[1]*

[1]*Department of Histology, Microbiology and Medical Biotechnology, University of Padova, Padua, Italy*
[2]*Department of Pharmaceutical Sciences, University of Padova, Padua, Italy*
[3]*Department of Biology, University of Padova, Padua, Italy*
[4]*INFM and Department of Physics, University of Genova, Genoa, Italy*
[5]*Division of Oncology and Hematology, Department of Pediatrics, University of Padova, Padua, Italy*

Previously, we have identified aloe-emodin (AE) as a new type of anticancer agent, with activity that is based on apoptotic cell death promoted by a neuroectodermal tumor-specific drug uptake. We attempt to clarify the intracellular target of AE and the apoptosis-signaling pathway activated by AE in neuroblastoma cell lines. Two-photon excitation microscopy and spectroscopic titrations documented that AE is highly concentrated in susceptible cells and binds to DNA. One of the most important mediators of apoptotic response to genotoxic stimuli, such as anticancer agents, is the p53 tumor suppressor gene. To evaluate the role played by p53 in AE-induced apoptosis a p53 mutant cell line, which lacks transcriptional activity of p53 targeted genes, was tested. AE displayed a reduced growth inhibitory and pro-apoptotic activity in p53 mutant cells (SK-N-BE(2c)) with respect to the p53 wild-type line (SJ-N-KP). This effect was not caused by a reduced drug uptake in the mutant neuroblastoma cell line but was related to a different apoptotic cell phenotype. Whereas SJ-N-KP cells were susceptible to a p53 transcription-dependent pathway of apoptosis, SK-N-BE(2c) cells underwent apoptosis with up-regulation of p53 expression but not of p53-target genes. After AE treatment p53 translocates to the mitochondria inter-membrane space in both neuroblastoma cell lines. Due to its high accumulation in neuroectodermal tumor cells AE could also kill tumor cells harboring p53 mutant genes. This property would further contribute to AE specific anti-tumor activity and might be exploitable in the clinic.

Key words: *aloe-emodin; anticancer activity and drug uptake; apoptosis; p53 nuclear and mitochondrial pathways; neuroblastoma*

Neuroblastoma is an embryonal tumor of the peripheral nervous system. It arises from the neural crest and is the most common solid extracranial tumor in infants, accounting for 10% of all childhood cancers. At the diagnosis about 50% of affected children have disseminated neuroblastoma disease.[1] Despite the array of chemotherapeutic agents available presently and current strategies employing intensive myeloablative chemotherapy, only 25% of patients with metastatic disease are long-term survivors over the age of 1 year.[2]

We have identified previously aloe-emodin (AE), a natural hydroxyanthraquinone, as a new antitumor agent against neuroectodermal tumors. We have described the selective *in vitro* and *in vivo* killing of neuroblastoma cells by AE. We have already demonstrated that anticancer activity of AE is based on apoptotic cell death, promoted by a tumor-specific drug uptake process in susceptible cells.[3]

Few cytotoxic drugs with different mode of action, including molecules with anthraquinone structure, have been found to induce programmed cell death.[4–7] One of the most important mediators of apoptosis is the p53 tumor suppressor gene, the central integrator of cellular response to stress stimuli, such as DNA damage, oncogenic signals, hypoxia and growth factor withdrawal.[8] In response to these stimuli p53 is stabilized, resulting in nuclear translocation and transactivation of numerous target genes.[9–11] Known p53 targets include genes involved in growth arrest (*p21* and *GADD45*) and apoptosis (*Bax*, *CD95*).[12–14] Although the exact mechanism of programmed cell death induction remains unknown it would likely involve, in the end stage, activation of the mitochondrial pathway. Accordingly different pro-apoptotic signals eventually provoke a change in mitochondrial integrity and the formation of the apoptosome.[15,16] This pathway results in cell dismantling with proteolysis of diverse cellular substrates, *i.e.*, poly(ADP-ribose)polymerase (PARP).[17]

The importance for p53-induced apoptosis in tumor suppression is further underlined by some tumor-derived p53 mutants. These mutants can acquire a selective loss of function for apoptosis[18] or have a gain of function phenotype,[19] manifested by augmented cell growth and tumorigenic potential.

Whatever p53 mutation can impact chemotherapeutic outcomes.[20–22] In this regard, different p53 mutants could be more or less responsive to a particular type of treatment. It is therefore important to define the functional differences between wild-type and mutant p53 to design rational therapeutic strategies that can selectively either restore wild-type tumor suppressor properties from mutant p53 or that can interfere with mutant p53 loss or gain of function activities.

The aim of our study was to clarify the intracellular target of AE and the apoptosis-signaling pathway activated by AE in neuroblastoma cell lines expressing a wild-type p53 gene or a transcriptionally deficient p53 mutant gene.

Abbreviations: AE, aloe-emodin; ATP, adenosine 5′-triphosphate; DTT, dithiothreitol; EGTA, ethyleneglycol-bis-(b-aminoethylether)-*N*,*N*,*N*′,*N*′-tetraacetic acid; IgG, immunoglobulin G; MIT, mitoxantrone dihydrochloride; MTT, 1-(4,5-dimethylthiazol-2-yl)-3,5-diphenylformazan; NP-40, Nonidet P-40; PARP, poly(ADP-ribose)polymerase; PI, propidium iodide; PMSF, phenylmethylsulfonyl fluoride; TEM, transmission electron microscope; TPE, two-photon excitation microscopy; VP-16, etoposide.

Grant sponsor: AIDS; Grant sponsor: MIUR; Grant sponsor: CNR; Associazione Italiana per la lotta al Neuroblastoma.

The first two authors equally contributed to this paper.

*Correspondence to: Giorgio Palù, Department of Histology, Microbiology and Medical Biotechnology, University of Padova, Medical School, via Gabelli 63; 35121 Padova, Italy. Fax: +39-049-8272355.
E-mail: giorgio.palu@unipd.it

Received 25 November 2002; Revised 21 March 2003; Accepted 25 April 2003

DOI 10.1002/ijc.11312

MATERIAL AND METHODS

Drugs

Aloe-emodin was purchased from Sigma-Aldrich (Italy) and was dissolved in DMSO, to reach a concentration of 200 mM and stored at −20°C. The compound was diluted in the appropriate medium immediately before use. Aloe-emodin is a fluorescent compound with a maximum excitation wavelength at 410 nm (λ_{ex}) and a maximum emission wavelength at 510 nm (λ_{em}). Mitoxantrone dihydrochloride (MIT) and etoposide (VP-16) were also purchased from Sigma-Aldrich. Pifithrin-α (PFTα) was purchased from Alexis (San Diego, CA).

Cell culture

Human neuroblastoma cell lines SJ-N-KP (with wild-type p53) and SK-N-BE(2c) with deficient p53 transcriptional activity (kindly provided by Paolo Montaldo, Gaslini Institute, Genova, Italy) and Ewing's sarcoma cells (TC106), were cultured in RPMI 1640 supplemented with 25 mM HEPES buffer and with 2 mM L-glutamine (all from Life Technologies, Ltd, Paisley. Scotland). SK-N-BE(2c) cell line derived from a neuronal clone of a bone marrow aspirate of a 2-year-old male patient when the tumor relapsed after treatment with doxorubicin, cyclophosphamide, vincristine and radiotherapy.[23] Primitive peripheral neuroectodermal tumor (pPNET) cell line (SK-PN-DW), human lung fibroblasts (MRC5), human hepatocellular carcinoma cell line (HepG2) and human cervix epithelioid carcinoma cell line (HeLa) were cultured in Dulbecco's modified Eagle's medium supplemented with 25 mM HEPES buffer and 2 mM L-glutamine (all from Life Technologies, Ltd, Paisley. Scotland). All culture medium were supplemented with 10% heat-inactivated FBS (Sigma-Aldrich, Milan. Italy), 100 U/ml penicillin and 100 μg/ml streptomycin (Sigma-Aldrich, Irvine. UK). All cell lines were grown at 37°C with 5% CO_2 humidified atmosphere.

Two-photon excitation microscopy

SJ-N-KP cells were seeded on microscope cover slips, in 12-well plates and cultured with drug-free medium 24 hr before treatment. Then AE was added at 5 μM of concentration. At 5 and 45 min AE uptake was analyzed with fluorescence two-photon excitation microscopy (TPE) in viable cells. Optical sections were acquired with a TPE architecture described in detail elsewhere.[24]

Specific AE cellular uptake

Aloe-emodin cellular uptake was carried out according to a published method.[25] In brief, SJ-N-KP, SK-N-BE(2c), HeLa and MRC5 cells were seeded in 60 mm dishes the day before and then incubated in complete drug-free medium or with AE 5 μM. After 5 and 45 min cells were washed twice in PBS to remove most of the free drug. Cells were then incubated with 0.3 N HCl in 50% ethanol for 15 min at 37°C; scraped and centrifuged for 5 min at 13,000*g*. The resulting supernatant was the cell-associated fraction. Aloe-emodin contents was evaluated by fluorometric readings using appropriate drug standard and drug-free control material for comparison. The λ_{ex} was 410 nm and the λ_{em} was 510 nm.

Fluorescent microscopy

SJ-N-KP cells were plated in 25-cm^2 flasks in complete medium. After an overnight incubation, cells were placed for 1 hr in medium with 5 μM AE. Cells were then washed twice in cold PBS and fixed with 1% paraformaldehyde for 15 min at 4°C as described previously.[26] After washing with cold PBS, cells were resuspended in 70% ethanol at 4°C and stored at −20°C until used. Cytospins were carried out with fixed cells resuspended in PBS. Cell nuclei were counterstained with 0.3 μg/ml propidium iodide (PI). Cytospins were examined under a Zeiss Axioplan microscope equipped with fluorescence lamps.

Spectrophotometric experiments

Spectrophotometric measurements were carried out in a Perkin-Elmer Lambda 5 instrument, equipped with a Haake F3C thermostat. According to a published method,[27] titrations were carried out at 25°C by addition of known amounts of double stranded calf thymus DNA to solutions containing a given concentration of the ligand (AE). Alternatively, known amounts of drug were added at constant DNA concentrations. Experimental binding data were evaluated according to the equation of McGhee and Von Hippel[28] for non-cooperative ligand-lattice interactions:

$$r/m = K_i(1 - nr)^n/[1 - (n - 1)r]^{n-1}$$

where r is the molar ratio of bound ligand to DNA, m is the free ligand concentration, K_i the intrinsic binding constant, and n the exclusion parameter.

Topoisomerase II cleavage assay

The plasmid pBR322 was cut at the EcoR1 site, and labeled by fill-in with the Large (Klenow) Fragment of DNA Polymerase I and [α-^{32}P]dATP. 0.1 μg of DNA were reacted with the indicated concentrations of drugs (0.1, 1 and 10 μM) and 2 U of human topoisomerase II-α (TopoGEN, Inc., Columbus, OH) at 37°C in 50 mM Tris-HCl (pH 8.0), 10 mM $MgCl_2$, 120 mM KCl, 0.5 mM DTT, 30 μg/ml BSA and 1 mM ATP. After 30 min of incubation at 37°C, samples were stopped by incubation with 0.5 mg/ml proteinase K and 1% SDS at 60°C for 3 hr, and then loaded on 1% agarose gel (0.09 M Tris-borate pH 8.3, 2.5 mM EDTA) and run for 16 hr at 40 volts. The gel was then dried and autoradiographed. DMSO or EtOH concentration was 1% in all samples.

Cell viability assays

The cytotoxic activity of AE was determined on exponentially growing cells in complete medium at 72 hr. Cells were plated in quadruplicate at a density of 5×10^3 cells per well, in 96-well plate. On the following day AE was added to the experimental final concentrations. Seventy-two hours later, cells were incubated with MTT dye (Cell Proliferation Kit I, Roche Diagnostics GmbH, Mannheim, Germany) according to the manufacturer's instructions. Optical density was determined by measuring absorbance at 550 nm. All experiments were conducted at least in triplicate.

FACS analysis

To evaluate the effect of AE on the cell cycle of neuroblastoma cell lines, 1×10^6 cells were cultured for different time periods in the presence of AE, of PFTα an inhibitor of the p53-dependent transcriptional activity, or in drug-free medium. After treatment cells were harvested, washed twice with PBS and fixed with cold 70% ethanol at 4°C. After centrifugation of the samples, PI (50 μg/ml in PBS) and RNAse were added to the pellet for 20 min at 37°C. DNA fluorescence was measured by flow-cytometry (EPICS XL, Coulter, Miami, FL) analysis according to a published method.[29]

Real time RT-PCR

The relative quantitative expression of some genes involved in cell cycle control and apoptosis was detected by real-time PCR combined with reverse transcriptase.

Cells were plated in 60 mm dishes in complete medium. The day after cells were treated for designated time points and harvested by trypsinization. Total RNA was extracted using the Qiagen Total RNA Kit (Qiagen S.p.A. Milan, Italy). After treatment with RNase-free DNase (Roche Diagnostics GmbH), 5 μl of total RNA were PCR amplified, after retrotranscription, using random primers (PE Applied Biosystem, Milan, Italy). The RT reaction was carried out on 100 μl of final volume in according to the manufacturer's instructions (PE Applied Biosystem). The real-time PCR reaction was carried out in 25 μl final volume utilizing 5 μl of cDNA, 0.2 μM of each specific primers (Table I), 0.6 mM (each) dNTPs, 100 mM KCl, 10 mM Tris-HCl, 20 mM EDTA, 10 mM $MgCl_2$, 0.03 U AmpliTaq Gold DNA polymerase and the SYBR-green reagents according to the manufacturer's instructions (PE Applied Biosystem). PCR reactions were cycled 40 times after an

TABLE I – SPECIFIC PRIMERS FOR REAL TIME RT-PCR

Oligonucleotide primers	Sequence	Product size (bp)
p53	5′-GCA CTG GTG TTT TGT TGT GG-3′ 5′-GTG GTT TCA AGG CCA GAT GT-3′	307
Bcl-2	5′-AGA TGT CCA GCC AGC TGC ACC TGA C-3′ 5′-AGA TAG GCA CCC AGG GTG ATG CAA GCT-3′	367
Bax	5′-AAG CTG AGC GAG TGT CTC AAG CGC-3′ 5′-TCC CGC CAC AAA GAT GGT CAC G-3′	366
$p21^{WAF1/CIP}$	5′-GAC ACC ACT GGA GGG TGA CT-3′ 5′-CAG GTC CAC ATG GTC TTC CT-3′	172
β-actin	5′-TCA CCC ACA CTG TGC CCA TCT ACG A-3′ 5′-CAG CGG AAC CGC TCA TTG CCA ATC G-3′	295[1]

[1]PE Applied Biosystem.

initial denaturation step (95°C, 10 min) according to the following parameters: denaturation at 95°C, 15 sec and annealing/extension at 60°C, 1 min in an ABI PRISM 7700 Sequence Detection system. To normalize the RNA amount of the extracted samples, a real-time PCR analysis of the human β-actin cDNA was carried out with TaqMan β-actin reagents (PE Applied Biosystem). Gene expression was measured by quantification of cDNA corresponding to the target gene relative to a calibrator sample serving as a physiological reference. The calibrator sample was the cDNA from the untreated cells. All quantification were also normalized to an endogenous control (β-actin) to account for the variability in the initial concentration, the quality of the total RNA and the conversion efficiency of the reverse transcription reaction. The relative quantification analysis of a target template in the samples requires the following data: i) the mean of the threshold cycle value (C_T, the cycle at which a statistically significant increase of fluorescent signal is first detected) for each sample; ii) the difference (ΔC_T) between the C_T values of the samples of the target gene and those of the endogenous control; iii) the difference ($\Delta\Delta C_T$) between the ΔC_T values of the sample for each target and the mean C_T value of the calibrator for that target. The relative quantification value is expressed as $2^{-\Delta\Delta CT}$. This method was validated by Applied Biosystem. In all PCR reactions melting curve analysis and agarose gel electrophoresis confirmed the specificity of the amplification product. The PCR products were run at 60 V for 2 hr on a 2% agarose gel stained with ethidium bromide and visualized by UV illumination. Primers were designed using the Primer 3 program (http://www-genome.wi.mit.edu/cgi-bin/primer/primer3.cgi). All experiments were conducted at least in triplicate.

Preparation of total cell lysates

Cells were seeded onto 10-cm plates and incubated with or without AE. After incubation, cells were washed once with cold PBS, scraped gently with a rubber policeman and collected by low-speed centrifugation. The collected cells were solubilized on ice in RIPA cell lysis buffer (50 mM Tris-HCl pH 7.4, 150 mM NaCl, 1 mM EDTA, 1% Igepal, 0.5% sodium deoxycholate, 0.1% SDS) supplemented with complete protease inhibitor cocktail tablet (Roche Diagnostics) followed by removal of DNA and cell debris by centrifugation at 14,000 rpm for 5 min at 4°C. The resulting supernatants were collected and frozen at −80°C.

Isolation of nuclear and cytosolic fractions

Cells were plated in 75 cm^2 flasks in complete medium and treated the day after for designated time points. Cells were washed twice with PBS, scraped using ice-cold PBS and centrifuged for 5 min at 450*g*. Cell pellets were resuspended in lysis buffer (50 mM Tris-HCl pH 8, 140 mM NaCl, 150 mM $MgCl_2$) and incubated on ice for 15 min; 10% Igepal solution was added to a final concentration of 0.6% and mixture was vortexed vigorously for 10 sec. Cell lysates were centrifuged for 30 sec at 10,000*g*; the resulting supernatant was the cytoplasmic fraction; nuclear pellets were resuspended in the same buffer and stored at −80°C.

Isolation of enriched mitochondrial fraction

Cells were plated in 75 cm^2 flasks in complete medium. After an overnight incubation, cells were treated for designated time points, harvested by trypsinization and spun down at 200*g* for 5 min. Cell pellets were washed once with fresh medium and once with ice-cold PBS. Cells were lysed in Mitobuffer (250 mM sucrose, 20 mM HEPES [pH 7.5], 1 mM EGTA, 1 mM EDTA, 10 mM KCl, 1.5 mM $MgCl_2$, 1 mM DTT, 0.1 mM PMSF, 2 μg/ml Leupeptin, 2 μg/ml Pepstatin, 2 μg/ml Aprotinin). Lysates were spun at 800*g* for 20 min at 4°C. The pellet contained nuclei and intact cells, whereas the supernatant was the cytosol including the mitochondria. The supernatant was then spun at 10,000*g* for 20 min at 4°C. The pellet contained an enriched mitochondrial fraction which was washed at least once with Mitobuffer and spun down again at 10,000*g*. The mitochondrial enriched pellet was lysed by incubation for 15 min in TNC buffer (10 mM Tris-acetate (pH 8.0), 0.5% NP-40, 5 mM $CaCl_2$, 1 mM DTT, 0.1 mM PMSF, 2 μg/ml Leupeptin, 2 μg/ml Pepstatin, 2 μg/ml Aprotinin) on ice. The supernatant was centrifuged at 16,000*g* for at least 20 min to remove residual mitochondria and stored at −80°C.

Western blot analysis

The total proteins extracted were quantified by the bicinchoninic acid assay with BSA as standard (BCA protein assay, Pierce, IL). Equal total protein of nuclear, cytosolic and mitochondrial protein fractions were subjected to Western blot analysis. Sample buffer was added to aliquots (25 μg of protein) of lysates that were boiled for 3 min and then resolved by 12.5% SDS-PAGE. The resolved proteins were transferred to PVDF membranes and immunoblotted with monoclonal Abs against p53 (DO-1), p21 (C-19), Bcl-2 (N-19) and Bax (N-20) (Santa Cruz Biotechnology, Santa Cruz, CA), CD95 (Oncogene, Boston, MA) and cytochrome *c* (BD Biosciences, San Jose, CA) and PARP (New England Biolabs, UK). The blots were washed and followed by detection with colorimetric detection system (Opti 4CN, BioRad Laboratories S.r.l., Milan, Italy).

Measurement of caspase enzymatic activity

Caspase activation was determined with a colorimetric "ApoAlert Caspase Assay Kit" following the manufacturer's instructions (Clontech, Palo Alto, CA). Briefly, after treatment of cells with 30 μM AE for the indicated time periods, cells were harvested, pelleted, and frozen on dry ice. Cell lysis buffer was added to the cell pellets, and protein concentration was determined by using Bradford analysis. A total of 150 μg of cell lysate was incubated with 5 μl of a 1 mM stock of the respective labeled substrate at 37°C for 1 hr.

This assay utilizes a synthetic tetrapeptide, (DEVD or IEVD), labeled with a colorimetric molecule,*p*-nitroaniline (*p*NA) as substrate. DEVD/IEVD-dependent protease activity was assessed by detection of the free *p*NA cleaved from the substrates. The release of the chromophore *p*-nitroaniline (pNA) was mea-

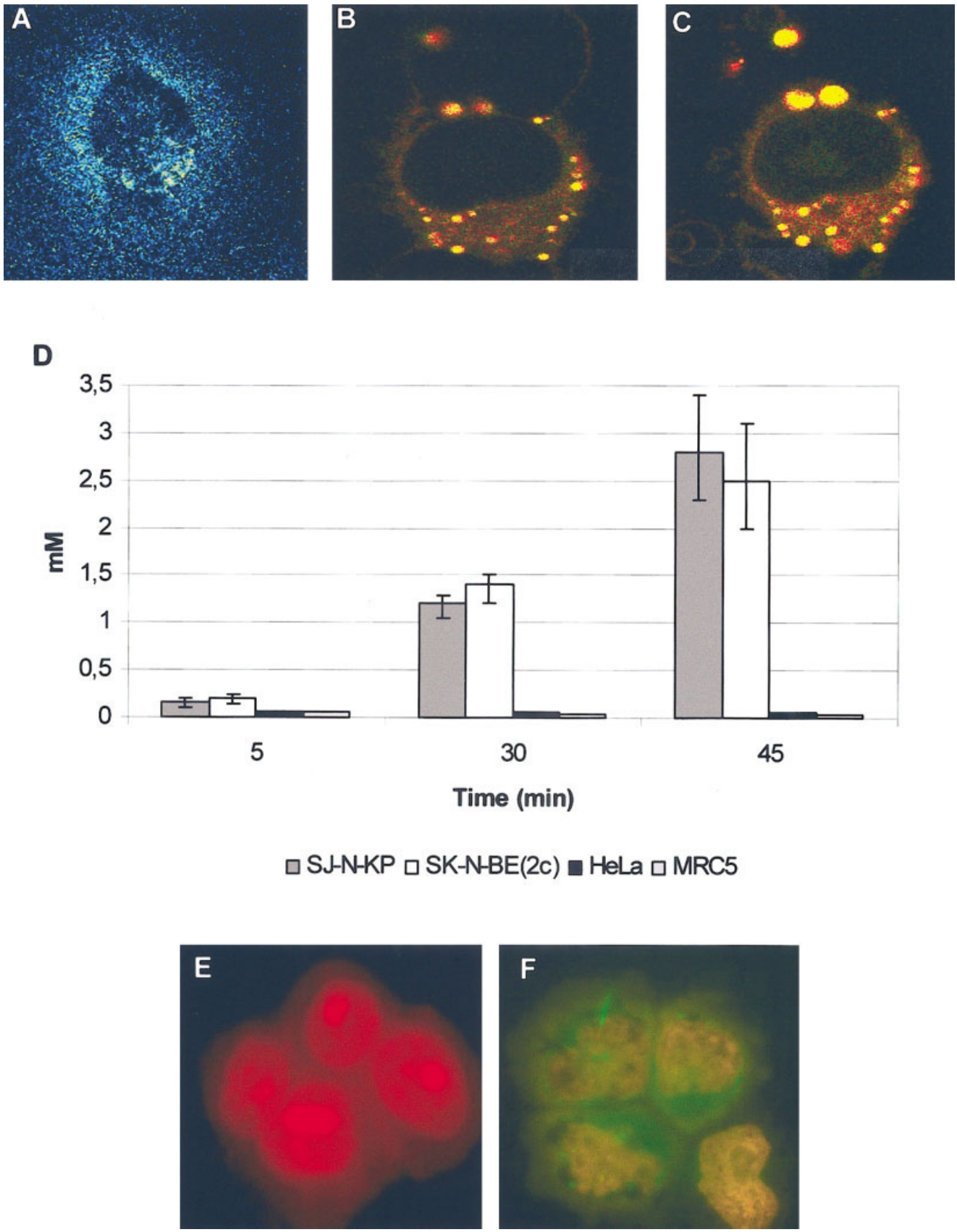

Figure 1 – Aloe-emodin intracellular distribution. Two-photon excitation analysis in neuroblastoma cells treated with AE 5 μM. SJ-N-KP cells in drug-free medium (*a*), after 5 min (*b*) and 45 min (*c*) of treatment. (*d*) Intracellular drug uptake by fluorometric analysis in neuroblastoma cells (SJ-N-KP and SK-N-BE(2c)), human cervix epithelioid carcinoma cells (HeLa) and normal fibroblast cells (MRC5) treated for the indicated time points with 5 μM of AE ($p < 0.05$). Fluorescent microscopy of PI-counterstained neuroblastoma cells nuclei (SJ-N-KP) after 1 hr of incubation without (*e*) or with AE 5 μM (*f*). The results are presented as the average ± SD of 3 experiments.

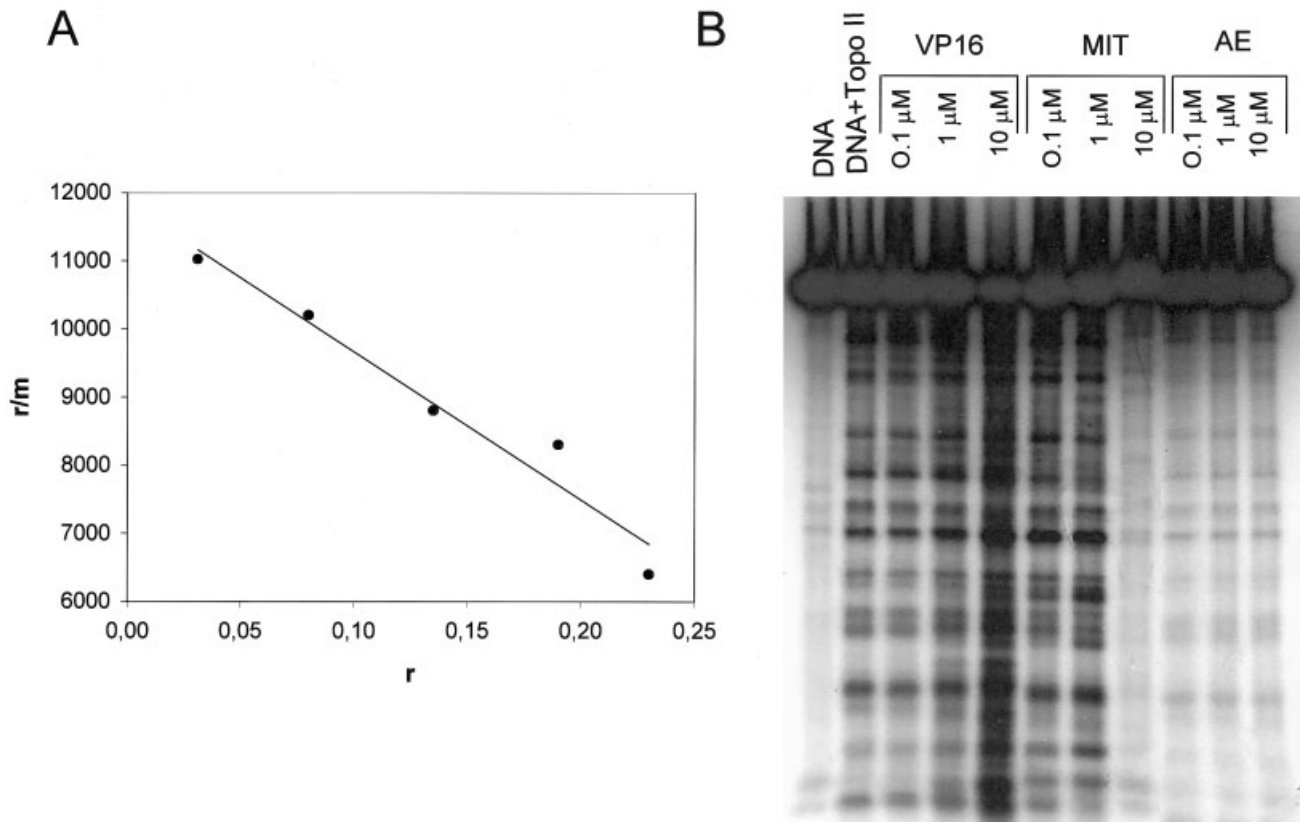

FIGURE 2 – Interaction of AE with DNA. (*a*) Scatchard plot for the binding of AE to Calf Thymus DNA. *r*, ratio between bound drug and total DNA on a phosphate basis; *m*, free drug concentration. (*b*) Topoisomerase IIa-dependent DNA cleavage stimulated by VP16, MIT and AE.

sured with a microplate reader (Spectra I, Tecan) at 405 nm. Caspase activities were assayed in duplicate samples. Caspase-8- and caspase-3-like enzymatic activities were assessed in parallel.

Immunoelectron microscopy

Cells were plated in 75 cm^2 flasks in complete medium. After an overnight incubation SJ-N-KP and SK-N-BE(2c) cell lines were treated with 30 μM AE or with drug-free medium. At designed time points cells were scraped, washed twice in PBS and fixed at room temperature for 2 hr, in 4% paraformaldehyde and 0.25% glutaraldehyde in PBS. Fixed cells were then processed for immunogold labeling according to a modified described method.[30] In brief, cells were dehydrated in ethanol and embedded in London Resin White. Ultrathin sections, cut with an Ultramicrotome (Ultracut, Reichert-jung), were picked up on nickel grids, washed with PBS, incubated for 1 hr in 1% BSA in PBS and treated with p53 (FL-393) polyclonal Ab (Santa Cruz Biotechnology). After washing with PBS, sections were incubated with secondary antibody IgG conjugated to 10 nm colloidal gold (Sigma-Aldrich, Italy) and observed with a transmission electron microscope (TEM 300, Hitachi) operating at 75 kV. Experiments without incubation of the primary antibody were carried out as control.

Statistical analysis

Statistical significance of the experimental results was determined by the Student's *t*-test.[31] For all analyses $p < 0.05$ was accepted as a significant probability level.

RESULTS

Aloe-emodin cellular uptake

The process of AE uptake in neuroblastoma cells was followed using two-photon excitation microscopy at concentrations close to ED_{50} values. Information was obtained on the relative amount of AE uptake and drug's intracellular fate in sensitive cells. In the first few minutes of incubation, AE staining moved from the plasma membrane to the cytoplasm of SJ-N-KP cells in a spotty fashion inside vesicles (Fig. 1*a–c*). As described in our previous work,[3] non-neuroectodermal tumor cell lines and human lung fibroblast were not susceptible to AE; in fact only a barely detectable fluorescence was noticed at concentrations up to 100 μM (data not shown). Fluorometric evaluation of cellular drug uptake was carried out to explain the relative amount of AE in susceptible cells compared to cervix epithelioid carcinoma cells (HeLa) and normal fibroblast cells (MRC5) (Fig. 1*d*). Our data indicate that AE is incorporated at high concentrations in both p53 wild-type (wt) and mutant (mut) neuroblastoma cells (Fig. 1*d*). In these cells intracellular molarities of 2.8–2.5 mM were reached after 45 min incubation with 5 μM AE. This represents an intracellular concentration process of 570-fold. The fluorometric signal in MRC5 and HeLa cells did not allow to appreciate a relative increase in drug uptake with time, suggestive of a membrane background value (Fig. 1*d*).

AE binding to DNA and nuclear localization

Having shown that AE is selectively incorporated in the cytoplasm of susceptible cells and knowing that AE-DNA interaction yields fluorescence quenching (not shown) and hypochromic effects (see below), nuclear components were evaluated as potential drug targets. PI counter-staining experiments (Fig. 1*e*) were conducted in intact cells to verify whether AE reached the nuclear compartment and bound to the chromatin structure. The orange emission from nuclei found at 1 hr post-AE treatment and immediately after PI addition, gave evidence that the two fluorochromes co-localized in this compartment (Fig. 1*f*).

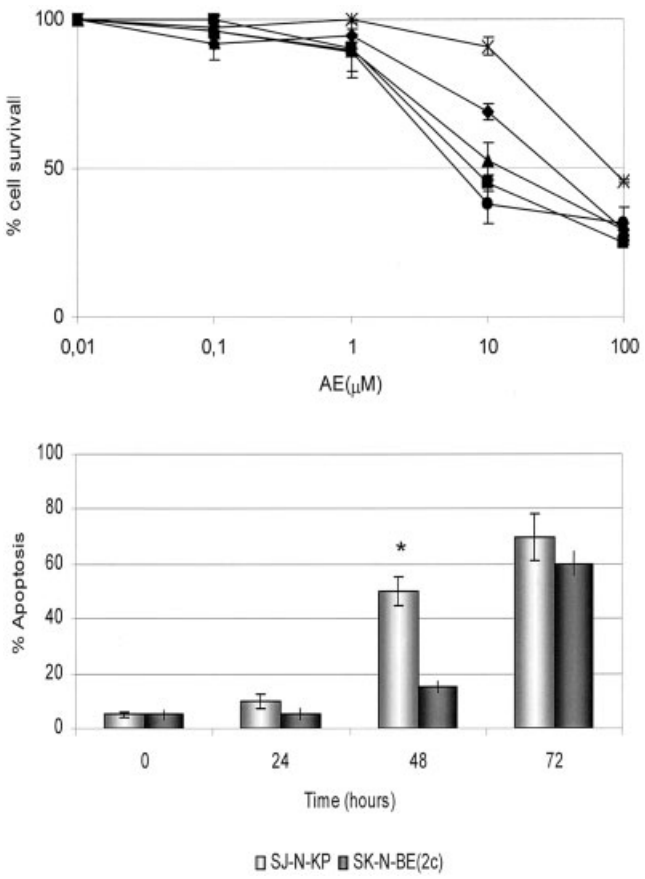

FIGURE 3 – (*a*) Aloe-emodin cytotoxicity. The cells were incubated with different concentrations of AE for a period of 72 hr. Toxicity dose-response curves were carried out on neuroectodermal and non-neuroectodermal tumor cell lines: SJ-N-KP (●), with wild-type p53, SK-N-BE(2c) (♦), a transcriptional-deficient p53 mutant, SK-PN-DW (▲), TC 106 (■) and HepG2 (✗). The fraction of viable cells was calculated by defining the viability of cells without treatment of AE as 100%. All determinations were made in triplicate. The results are presented as the average ± SD. (*b*) Effect of AE on cell-cycle dynamics determined by flow-cytometry. DNA content of 10,000 nuclei was assessed and mean values ± SD of percentages of nuclei with DNA content below 2n (sub-G_0 fraction) of 3 experiment are given. *$p \geq 0.05$.

Spectrophotometric drug titration techniques were carried out to characterize the interaction of AE with DNA, using conditions close to the active ones. Substantial spectral modifications were observed upon addition of the polynucleotide to buffered solutions of the examined drug. A red shift of the maximum absorption occurred, along with hypochromicity for the drug (data not shown). From the observed spectroscopic changes it was possible to evaluate the concentration of free and DNA-bound drug. The results were reported as a Scatchard plot in Figure 2*a*. The number of base pairs involved in the complex formation is close to 2 and the binding constant is about 12,000 M^{-1}.

Inhibition of topoisomerase II activity

Many known Topo II inhibitors, including anthracycline derivatives bind non-covalently to DNA and poison the enzyme by inhibiting the DNA resealing reaction after double stranded nucleic acid cleavage.[32,33] Activation of DNA cleavage is the consequence. The ability of AE, VP16 and mitoxantrone in stimulating double-stranded DNA breaks in the presence of purified human topoisomerase IIα (Fig. 2*b*) was evaluated. Radioactively labeled DNA fragments were used in this assay, and cleavage sites were mapped by agarose gel electrophoresis. As expected on the basis of previous studies[34,35] the cleavage efficiencies of mitoxantrone and VP16 were high. On the other hand, AE did not stimulate double-stranded DNA breaks formation but rather inhibited this activity.

Specific cytotoxicity of AE for neuroblastoma cells

The cytotoxic potential of AE was evaluated on exponentially growing cells over a period of 72 h. Cells were cultured in drug-free medium or in the presence of increasing AE concentrations. AE displayed a specific dose-dependent cytotoxic effect on many neuroectodermal tumor cell lines, *i.e.*, neuroblastoma, Ewing sarcoma and pPNET cells with ED_{50} values (half-maximal effective doses) ranging from 4.2 ± 1 μM and 29.1 ± 2.5 μM (Fig. 3*a*). In particular SJ-N-KP cells expressing a wild-type p53 were more sensitive to AE than SK-N-BE(2c) cells, which exhibit a p53 loss of transcriptional activity. ED_{50} values range between 4.2 ± 1 μM and 29.1 ± 2.5 μM, respectively. The effect of AE on the cell cycle of neuroblastoma cells exhibited apoptosis induction in both cell lines. In SJ-N-KP (the wild-type p53 cell line) programmed cell death appeared earlier than in SK-N-BE(2c) (the mutant p53 cell line) (Fig. 3*b*).

Effects on mRNA expression of p53 and its target genes

Having found that AE kills neuroblastoma cells, both with wild-type *p53* and with transcriptionally deficient *p53*, we evaluated the effects of this compound on the expression of some genes involved in the cell cycle regulation and apoptosis. The relative quantitative expression of these genes was detected by real-time PCR combined with reverse transcriptase. SJ-N-KP and SK-N-BE(2c) cells were treated with a concentration of 5 μM and 30 μM AE respectively (Fig. 4). Treatment with AE induced a time-dependent increase of mRNA-expression of *p53* in both SJ-N-KP and in SK-N-BE(2c) cells (Fig. 4*a*). p21, Bcl-2, Bax and CD95 mRNA levels started to increase at 12 hr post AE-treatment in SJ-N-KP cells (Fig. 4*b–e*). Conversely there was no transactivation of p53-target genes, such as p21, Bax, Bcl-2 and CD95 (Fig. 4*b–e*) in SK-N-BE(2c) cells; these results are consistent with loss of function for p53 in this mutant cell line.[23] All studied genes were considered significantly induced when the induction ratio (I.R.) was ≥2.0.

Effects of AE on cell cycle regulators and apoptosis-related proteins expression

Western blot analysis was carried out after treatment of SJ-N-KP and SK-N-BE(2c) cells for the indicated time-points in the range of their respective ED_{50} values. These ED_{50} concentrations were used to appreciate the real apoptotic phenotype of mutant and wild-type p53 cells. Our data showed that there was a time-dependent increase of p53 protein in both cell lines (Fig. 5). p53 protein level, in the nuclear fraction, began to rise at 12 hr in SJ-N-KP cells and at 36 hr in SK-N-BE(2c) cells. An increase in the p21 and CD95 protein levels occurred at a later time point, in SJ-N-KP cells. There was no induction in p21 and CD95 protein expression in SK-N-BE(2c) cells. Moreover there was no induction of CD95L protein in both cell lines (data not shown). A translocation of Bax protein to the mitochondria was observed in both neuroblastoma cell lines, as shown by the increase of Bax levels in mitochondria enriched fraction. An increase of Bcl-2 protein was also observed in the mitochondria enriched fraction of both cell lines (Fig. 5*a*,*b*).

Cytochrome c *release and proteolytic cleavage of PARP*

The release of cytochrome *c* from the mitochondria inter-membrane space into the cytosol is a prominent downstream manifestation of the evolution of apoptotic cell death.[16,36] To assess whether p53 activates the apoptosome by inducing cytochrome *c* release, a subcellular fractionation of neuroblastoma cells was carried out at various time-points after AE treatment. Cytochrome *c* release into the cytosolic fraction of SJ-N-KP cells began to rise

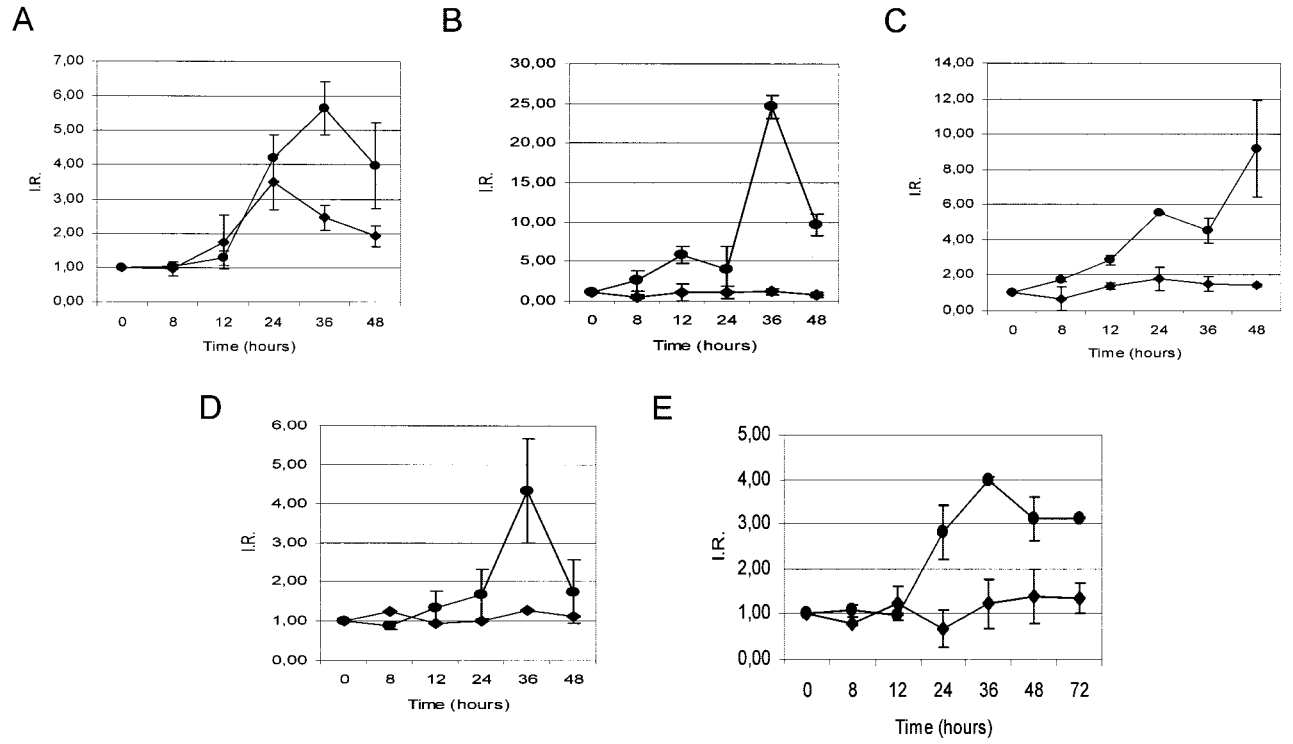

FIGURE 4 – Real-time RT-PCR analysis of p53 (*a*), p21 (*b*), bcl-2 (*c*), bax (*d*) and CD95 (*e*) gene expression in neuroblastoma cell lines. SJ-N-KP (●) and SK-N-BE(2c) (♦) cells were treated with 5 and 30 μM of AE respectively, for the designated time points. The results were expressed as induction ratio (I.R.) referred to the control levels of gene expression. The experiments were conducted, at least, in duplicate. I.R. $\geq$ 2.0 was considered significant.

at 8 hr, together with a decrease in the cytochrome *c* content in the mitochondria enriched fraction (Fig. 6*a*, upper panel). Release into the cytosol began to rise at 24 hr, in SK-N-BE(2c), and a decrease in the cytochrome *c* content is also evident in the mitochondria enriched fraction (Fig. 6*b*, upper panel). Cleavage of PARP, a substrate of caspase 3, was detected at 24 hr in SJ-N-KP cells (Fig. 6*a*, lower panel) and at 36 hr in SK-N-BE(2c) cells (Fig. 6*b*, lower panel).

Caspase 3 and 8 activity

To identify whether AE induced apoptosis involved caspases pathway we assessed the activation of caspases-3 and -8 by colorimetric assay in cultured cells. Both cell lines were treated, at different time-points, with 30 μM AE. Caspase-3-like enzymatic activity increased at 24 hr in SJ-N-KP cells (Fig. 7*a*) and at 36 h in SK-N-BE(2c) (Fig. 7*b*); conversely there was no induction of caspase-8 activity in both cell lines.

Effects of pifithrin-α on the sensitivity of neuroblastoma cells to AE

PFTα is a small molecule that was isolated for its ability to reversibly block p53-dependent transcriptional activation.[37] We used this compound to investigate whether a p53 transcription-dependent pathways was involved in AE-apoptosis induction. FACS analysis was conducted on wt- and mut-p53 cell lines. Cells were pretreated with PFTα 30 μM for 18 hr and then treated with 30 μM AE for 48 hr. As shown in Figure 7*c*, a significant decrease in the number of apoptotic cells, indicative of a reduction in the sensitivity of SJ-N-KP cell line to AE, was observed. There was no difference in the number of apoptotic cells in SK-N-BE(2c) cell line, as an indication for a different apoptotic cell phenotype. Whereas SJ-N-KP cells were susceptible to a p53 transcription-dependent pathway of apoptosis, SK-N-BE(2c) cells underwent apoptosis with up-regulation of *p53* expression but not of p53-target genes.

AE-induction of mitochondria p53 accumulation

SK-N-BE(2c) cells, although carrying a missense mutation at codon 135 of exon 5 of p53 gene (part of the DNA-binding domain essential for p53 transcriptional activity)[23] remain relatively sensitive to AE-induced apoptosis (Fig. 3). Because p53 has been shown to possess a transcription-independent action involving mitochondria,[38–41] the possibility of p53 translocation to these organelles was investigated in SK-N-BE(2c) cells. Western blot analysis on mitochondria enriched fractions of SJ-N-KP and SK-N-BE(2c) cells were carried out after 30 μM AE treatment. This concentration was used to verify if p53 mutant cells behave differently from wild-type ones under similar conditions of drug exposition. A scarce presence of p53 in the mitochondria and no increase in the cytosol was observed in SJ-N-KP cells (Fig. 8*a*). Conversely the level of p53 protein increased both in the mitochondria and in the cytosol, post-AE treatment, in SK-N-BE(2c) cells (Fig. 8*f*). Immuno-electron microscopy was carried out to evaluate the presence of p53 protein in intact cells and to verify whether p53 traffics from the cytosol to the mitochondria. Staining was quantified by randomly selecting 50 fields. Whereas p53 appeared poorly abundant in mitochondria of SJ-N-KP cells (Fig. 8*c*,*e*), a more intense labeling was present in the same subcellular fraction of SK-N-BE(2c). Grains preferentially localized on the mitochondria cristae (Fig. 8*h*,*l*). Only background was obtained in untreated cells (Fig. 8*b*,*g*). The p53 mitochondrial localization in SK-N-BE(2c) cells, as shown by immunoblotting (Fig. 8*f*), precedes cytochrome *c* release into the cytosol (Fig. 6*b*). These findings support a role of the p53 protein in direct apoptotic signaling at mitochondria, as supported previously.[38] There is no evidence of such a pathway in SJ-N-KP cells.

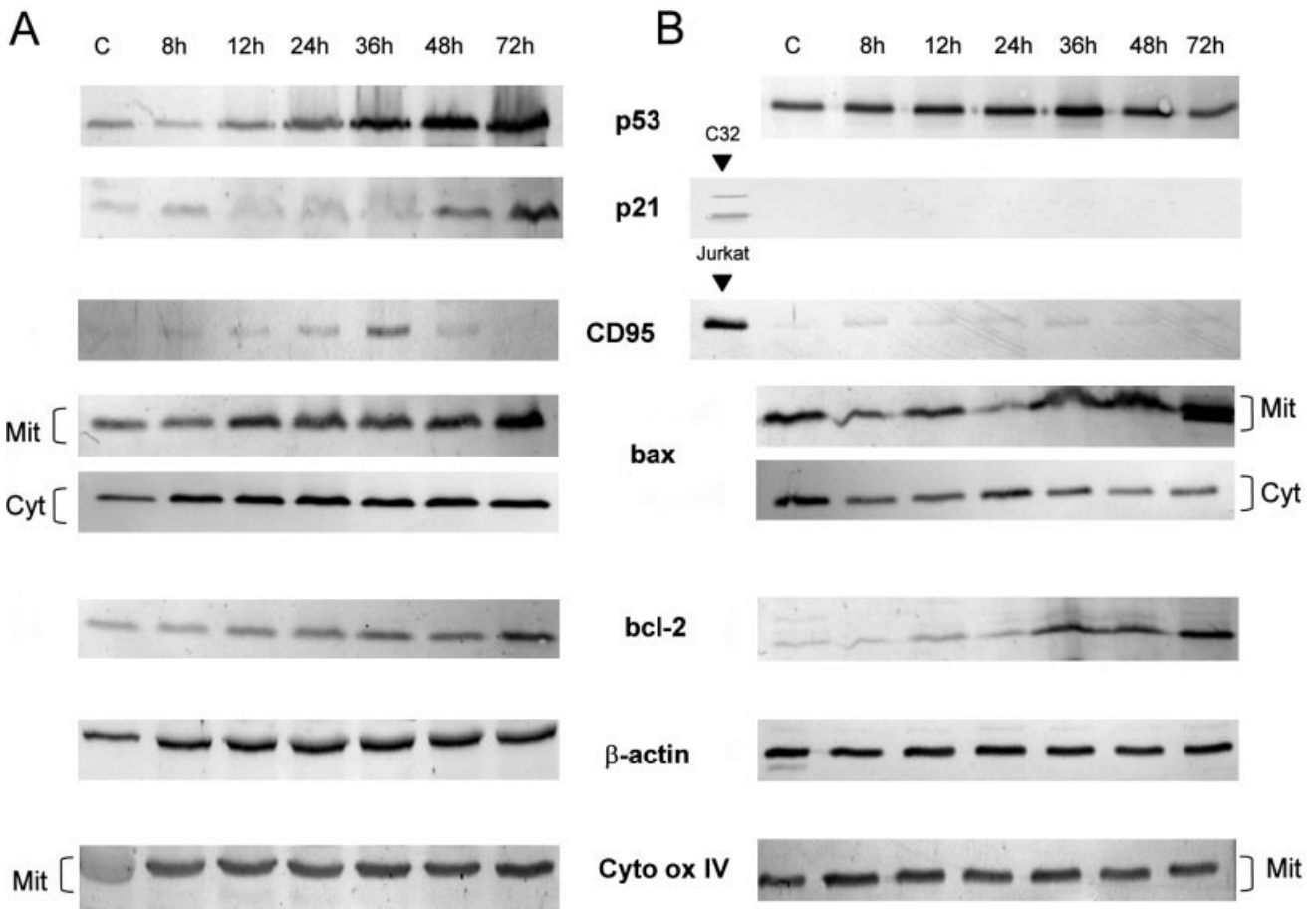

FIGURE 5 – Western blot analysis in neuroblastoma cells (30 μg of protein per lane in all subfigures). The analyses were carried out for SJ-N-KP (*a*) and SK-N-BE(2c) (*b*) after treatment with 5 and 30 μM of AE respectively. p53 and p21 proteins were analyzed in the nuclear fractions. CD95 protein was detected in all cellular lysates. Bax was detected in cytosolic (Cyt) and mitochondrial enriched (Mit) fractions and Bcl-2 was detected in the mitochondrial enriched fraction. *C32*, positive control for p21 protein in SK-N-BE(2c) cells; *Jurkat*, positive control for CD95 protein in SK-N-BE(2c) cells; *C*, untreated cells. β-Actin validates equal gel loading and cytochrome oxidase IV (*cyto ox IV*) is a mitochondrial marker.

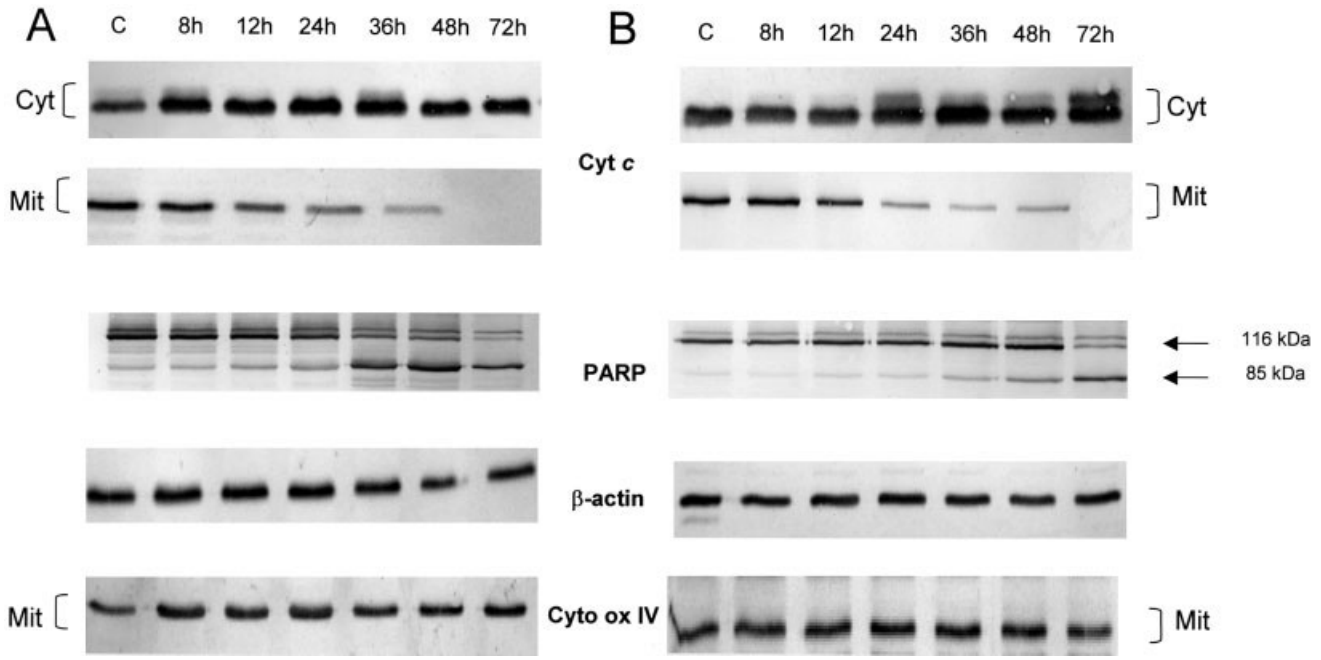

FIGURE 6 – Immunoblots (30 μg of protein per lane) in cytosolic fraction of neuroblastoma cells for cytochrome *c* (Cyt c) relapse from mitochondria and PARP cleavage. Cytochrome *c* was also detected in mitochondrial enriched fraction (Mit). The analyses were carried out in SJ-N-KP (*a*) and SK-N-BE(2c) (*b*) after treatment with 5 and 30 μM of AE respectively. *C*, untreated cells β-actin validates equal gel loading and cytochrome oxidase IV (*cyto ox IV*) is a mitochondrial marker.

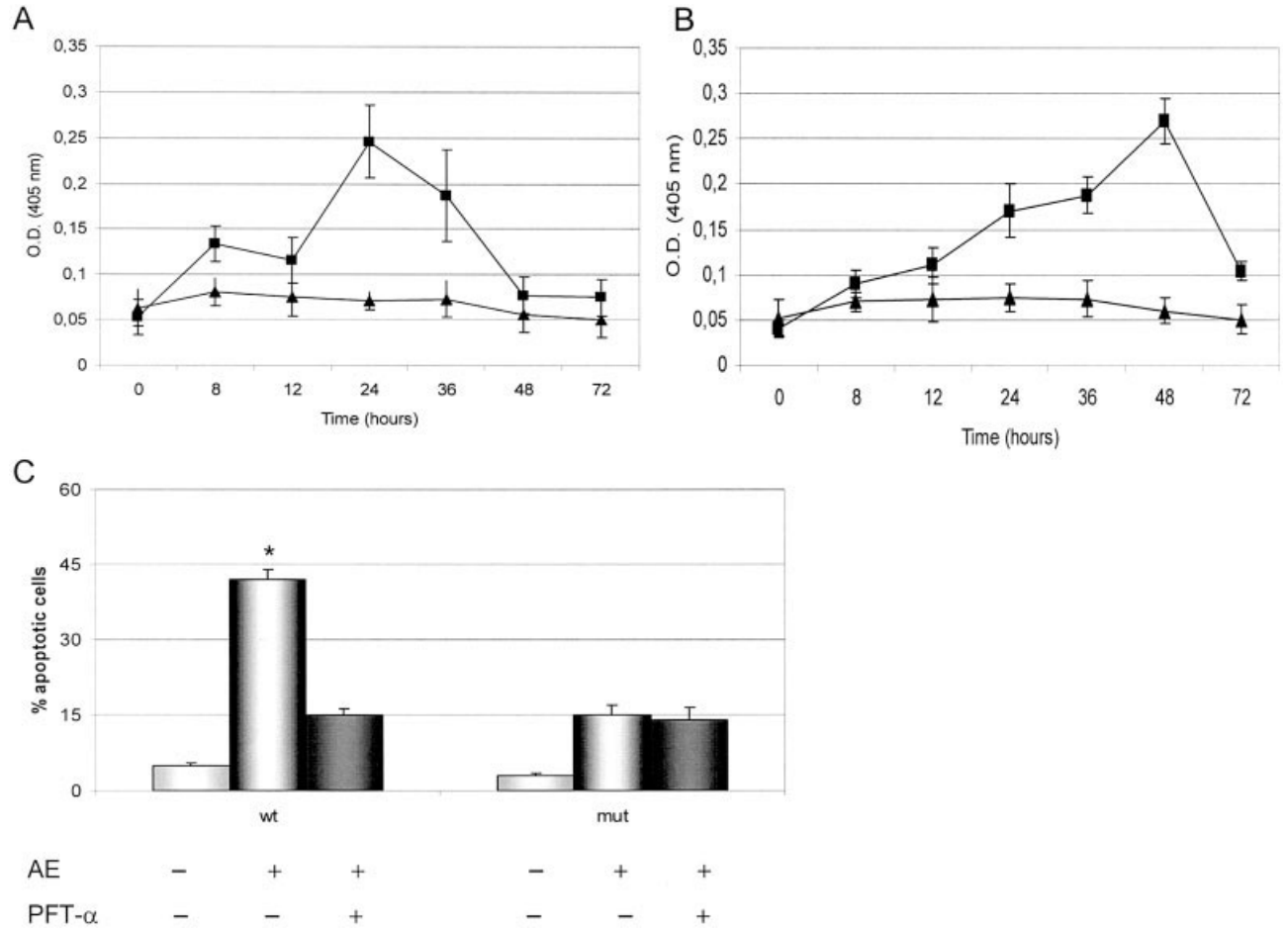

FIGURE 7 – (*a*,*b*) Kinetics of AE-induced caspases activation. SJ-N-KP (*a*) and SK-N-BE(2c) (*b*) cells were treated with 30 μM for the indicated times; cell lysates were made, and caspase-8 and caspase-3-like enzymatic activities were measured by hydrolysis of IETD-pNA and DEVD-pNA, respectively. The experiments were conducted, at least, in duplicate. The results are presented as the average ± SD (*$p \geq 0.05$). (*c*) Inhibitory effect of PFTα on AE-induced apoptosis in neuroblastoma cell lines. DNA content of 10,000 nuclei was measured by flow cytometry and mean values ± SD of percentages of nuclei in sub-G_0 phase of 3 independent experiment are given. *$p \geq 0.05$.

DISCUSSION

We have demonstrated in a previous work[3] that AE is a new type of anticancer agent. Its activity is based on apoptotic cell death promoted by a neuroectodermal tumor-specific drug uptake with lack of appreciable toxicity for dividing normal host tissues.

We have identified the intracellular target of AE and the apoptosis-signaling pathway that AE activates in susceptible neuroblastoma cells.

Other groups, including ourselves, investigated AE as a cytotoxic agent on non-neuroectodermal tumor cell lines, namely leukemia, hepatoma, colon adenocarcinoma, cervix epithelial carcinoma and lung carcinoma cell lines.[3,42–44] The ED_{50} values that were reported for those cell lines were much higher (40–100 μM AE) than those for neuroectodermal tumor cells (1–13 μM). The mode of drug uptake must certainly be crucial to explain the nature and specificity of AE cytotoxicity for neuroblastoma cells shown to rely upon a temperature and energy dependent process.[3] Experiments of TPE microscopy were therefore carried out to follow fate and intracellular distribution of AE in susceptible cells. Early after incubation with an AE concentration near the ED_{50} (5 μM), the drug was incorporated prevalently into a vesicular compartment, a finding suggestive of an endocytic pathway. By contrast, fluorescence emission was barely detectable in HeLa cells[3] and MRC5 cells maintained under the same experimental conditions (data not shown). Fluorometric evaluation of drug uptake by neuroblastoma cells allowed to appreciate that AE is concentrated intracellularly by over 500-fold compared to the extracellular concentration of the molecule. This is further evidence suggesting the occurrence of an active transport process that might involve endocytosis via an as yet uncharacterized receptor. As shown by co-localization experiments, the anthraquinone already interacts with the nuclear components of neuroblastoma cells at 1 hr post-treatment. Such a nuclear localization of AE was not manifest in non-neuroectodermal tumor cells. Spectroscopic titrations documented that AE binds to DNA with an intrinsic binding constant value (12,000 M^{-1}) that compares favorably with the one reported for other DNA-targeted drugs like *m*-AMSA.[45] At variance with other anthraquinone[32,33] AE did not behave as a DNA topoisomerase II poison, as measured by induction of nucleic acid cleavage. Another group reported that high doses of AE inhibited cleavage rather than stabilizing the DNA-enzyme cleavage complex, a finding consistent with Topo II-competition of AE for DNA binding.[46] The high concentration reached by AE in susceptible cell lines (about 2 mM) together with the considerable affinity for DNA suggests that a large part of the drug should be bound to DNA in the nucleus, where AE can efficiently interfere with chromatin structure and DNA template functions. In response to DNA damage the cellular levels of p53 are greatly increased. Apoptosis

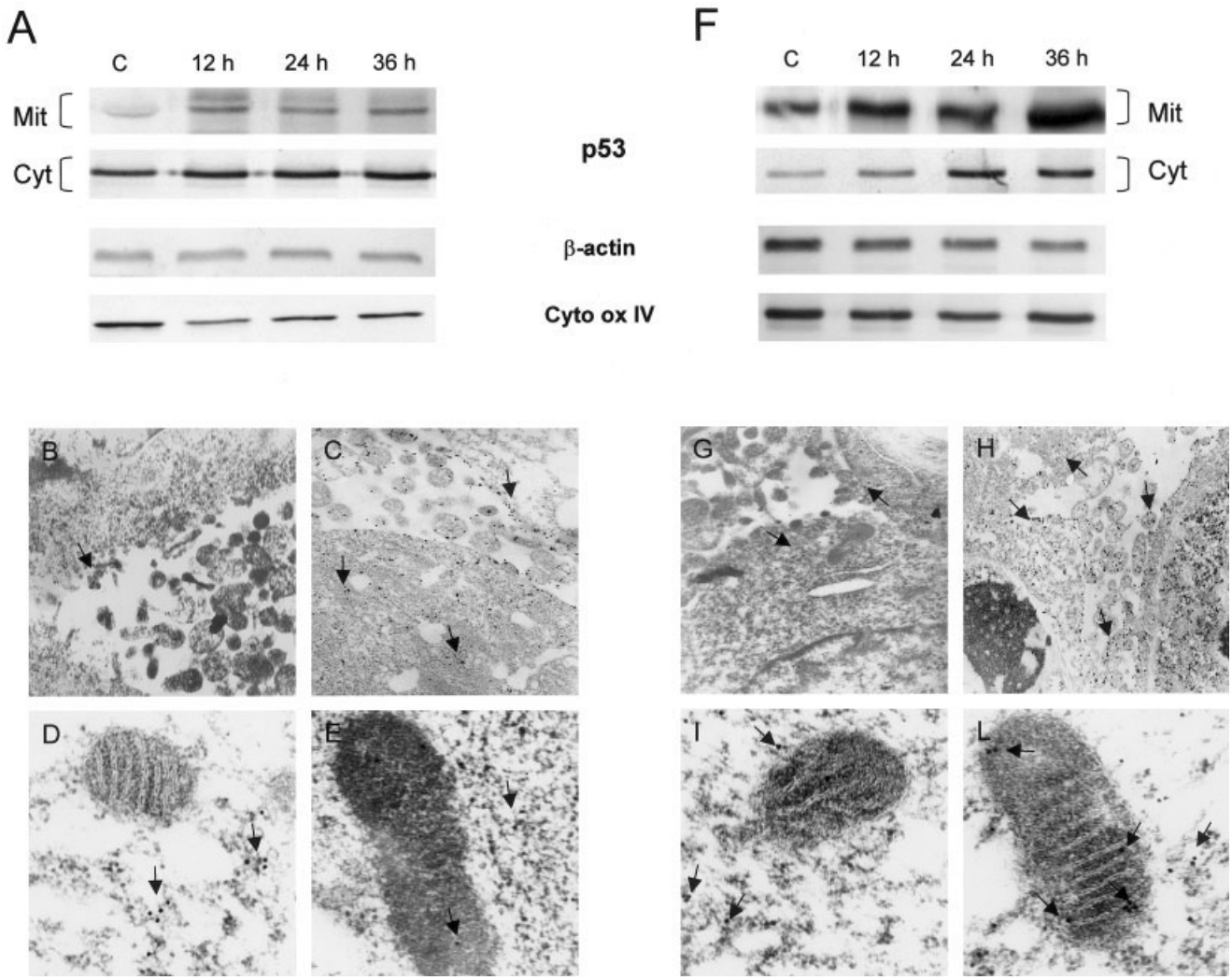

FIGURE 8 – Kinetics and localization of mitochondrial p53. (*a*,*f*) Immunoblots (30 μg of protein per lane) of mitochondrial enriched (Mit) and cytosolic (Cyt) fractions of SJ-N-KP and SK-N-BE(2c) after treatment with 5 and 30 μM of AE respectively. *C*, untreated cells. β-Actin validates equal gel loading and cytochrome oxidase IV (*cyto ox IV*) is a mitochondrial marker. Immunoelectron microscopy of p53 protein in mitochondria of SJ-N-KP and SK-N-BE(2c) treated cells with 30 μM AE. (*b–e*) SJ-N-KP cells. (*g–l*) SK-N-BE(2c) cells. Untreated cells 20,000× (*b*,*g*) and 62,000× (*d*,*i*). Cells after adding AE 20,000× (*c*,*h*) and 62,000× (*e*,*l*). p53 immunogold staining is indicated by the arrows.

described at high drug concentrations in AE-insensitive tumor cells[42–44] could rest on the effects produced at the plasma membrane level by a rather lipophilic molecule (evaluated log P of about 4.1).

The mechanism of p53-mediated apoptosis remains still unclear. In particular, it remains controversial as to whether p53 transcriptional activity is also necessary for p53-dependent apoptosis. From current understandings, there are two p53-dependent pathways of inducing programmed cell death,[47,48] the "intrinsic" and the "extrinsic" pathway, characterized by caspase activation with or without involvement of mitochondria, respectively. The extrinsic pathway is initiated through engagement of cell surface death receptors that lead to caspase-8 activation (such as CD95, TNFR1 and TRAIL, by their respective ligands).[6,7] The intrinsic pathway is regulated by the pro-apoptotic Bcl-2 family proteins (*i.e.*, Bax), that induce the release of apoptogenic factors, such as cytochrome *c*, from the mitochondrial intermembrane space into the cytosol. Cytochrome *c* release initiates formation of apoptosome, a complex that includes procaspase-9, dATP and Apaf-1.[15] In both the death receptor/caspase-8 and the mitochondria/caspase-9 pathways, the eventual activation of effector proteases caspases 3,6 and 7 results in dismantling of the cell as diverse cellular substrates are proteolyzed, *i.e.*, poly(ADP-ribose)polymerase (PARP).[17]

In our experimental system we found that AE induced the intrinsic pathway while failing to induce the extrinsic pathway, as no CD95 involvement and no caspase-8 activation were observed.

To evaluate the role played by *p53* in AE-induced apoptosis, and to further confirm the genotoxic activity of intracellularly accumulated AE, a p53 mutant cell line that lacks transcriptional induction of p53 targeted genes was tested. This abnormality in the p53 tumor suppressor gene pathway is one of the most important mechanisms of chemo- and radio-resistance in many tumor cells.

Our data showed that the induction of apoptosis by AE in mutant p53 was slower than that induced in wt p53 cell lines. This effect was not caused by a lowered drug uptake in the mutant neuroblastoma cell line but was related to a different apoptotic cell phenotype. SJ-N-KP cells were susceptible to a p53 transcription-dependent pathway of apoptosis, as confirmed by a consistent reduction in apoptosis after treatment with PFT-α. Instead, SK-N-

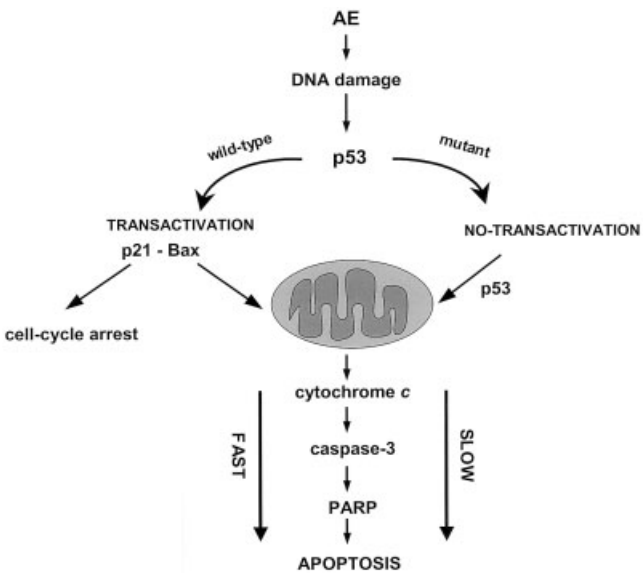

FIGURE 9 – A model for summarizing AE-induced p53-dependent apoptosis pathways in neuroblastoma cell lines.

BE(2c) cells underwent apoptosis with upregulation of p53 protein level and without induction of p53-target genes. In both cell lines release of mitochondrial cytochrome *c* into the cytoplasm occurred with caspase-3 activation and PARP cleavage.

Because mutant p53 lacks measurable transactivation potential, our findings suggest the existence of two p53 dependent-apoptotic pathways: one involves activation of specific target genes and the other is independent of it.

Evidence for a transcription-independent pattern of p53-mediated apoptosis has been recently accumulating.[38–41] The mechanistic process involved would rely upon movement of a fractional amount of p53 to the surface of mitochondria in response to death signals from anticancer drugs and hypoxia.[38,39] By doing so, p53 would normally contribute to apoptosis by direct signaling at the mitochondria.

We show that p53 translocates to the mitochondria inter-membrane space, close to the cristae, in both neuroblastoma cell lines at variance with a previous report[38] where an association to the mitochondria membranous compartment was described. This is unlikely to be an artifact because mitochondria localization in SK-N-BE(2c) cells precedes cytochrome *c* release into the cytosol. Moreover, for the first time, activation of a transcription-independent pathway of p53-mediated apoptosis is described in a *p53* transcriptionally deficient cell line. It is therefore reasonable to assume that the higher ED_{50} exhibited by the mutant neuroblastoma cell line depends from the fact that apoptosis is caused solely by the p53 direct mitochondrial pathway, that is less efficient than the classical pattern. This assumption is substantiated by a delayed cytochrome *c* release and PARP cleavage in mutant cells (Fig. 6).

In conclusion, we propose a model explaining pronounced AE cytotoxicity in neuroblastoma cell lines. After a selective uptake the molecule is concentrated in the nucleus of susceptible cells where it can efficiently bind chromatin as a result of high drug/DNA ratios. This extensive interaction is likely sufficient to impair many DNA functions. As a consequence, p53 becomes alerted and, once stabilized, can trigger an apoptotic cellular response, via both a transcriptional dependent and independent pathway (Figure 9). Due to its high accumulation in neuroectodermal tumor cells (mM range) AE could also kill tumor cells harboring p53 mutant genes. This property would further contribute to AE specific anti-neuroectodermal tumor activity and might be exploitable in the clinic, thanks to a safe toxicology record and a good pharmacokinetic profile of AE, as emerged from our preliminary animal models. Identification of the transporter system that affords selective toxicity to a drug with a non-selective target, such as DNA, may prompt genetic manipulations aimed at treating AE-insensitive tumors.

ACKNOWLEDGEMENTS

The authors wish to thank G. Basso and M. Pizzato for suggestions and assistance. Financial support from AIDS grant, MIUR grant, CNR grant (to G.P.) and from Associazione Italiana per la lotta al Neuroblastoma (to T.P.) is also acknowledged. This work is dedicated to Giada.

REFERENCES

1. Brodeur GM, Castelberry RP. Neuroblastoma. In: Pizzo PA, Poplack DG, eds. Principles and practice of pediatric oncology. Philadelphia: J.B. Lippincott Co., 1997. 761–97.
2. Tweddle DA, Pinkerton CR, Lewis IJ, Ellershaw C, Cole M, Pearson AD. OPEC/OJEC for stage 4 neuroblastoma in children over 1 year of age. Med Pediatr Oncol 2001;36:239–42.
3. Pecere T, Gazzola MV, Mucignat C, Parolin C, Dalla Vecchia F, Cavaggioni A, Basso G, Diaspro A, Salvato B, Carli M, Palù G. Aloe-emodin is a new type of anticancer agent with selective activity against neuroectodermal tumors. Cancer Res 2000;60:2800–04.
4. Sartorelli AC, Laso JS, Bertino JR, eds. Molecular actions and targets for cancer chemotherapeutic agents. New York: Academic Press, 1981.
5. Barry MA, Behnke CA, Eastman A. Activation of programmed cell death (apoptosis) by cisplatin, other anticancer drugs, toxins and hyperthermia. Biochem Pharmacol 1990;40:2353–62.
6. Mitsiades N, Mitsiades CS, Poulaki V, Chauhan D, Richardson PG, Hideshima T, Munshi NC, Treon SP, Anderson KC. Apoptotic signaling induced by immunomodulatory thalidomide analogs in human multiple myeloma cells: therapeutic implications. Blood 2002;99: 4525–30.
7. Szmigielska-Kaplon A, Smolewski P, Najder M, Robak T. Evaluation of apoptosis induced in vitro by cladribine (2-CdA) combined with anthracyclines in lymphocytes from patients with B-cell chronic lymphocytic leukemia. Ann Hematol 2002;81:508–13.
8. Levine AJ. p53, the cellular gatekeeper for growth and division. Cell 1997;88:323–31.
9. An WG, Kanekal M, Simon MC, Maltepe E, Blagosklonny MV, Neckers LM. Stabilization of wild-type p53 by hypoxia-inducible factor 1alpha. Nature 1998;392:405–8.
10. Kastan MB, Onyekwere O, Sidransky D, Vogelstein B, Craig RW. Participation of p53 protein in the cellular response to DNA damage. Cancer Res 1991;51:6304–11.
11. Budihardjo I, Oliver H, Lutter M, Luo X, Wang X. Biochemical pathways of caspase activation during apoptosis. Annu Rev Cell Dev Biol 1999;15:269–90.
12. Prives C, Hall PA. The p53 pathway. J Pathol 1999;187:112–26.
13. May P, May E. Twenty years of p53 research: structural and functional aspects of the p53 protein. Oncogene 1999;18:7621–36.
14. Han J, Sabbatini P, Perez D, Rao L, Modha D, White E. The E1B 19K protein blocks apoptosis by interacting with and inhibiting the p53-inducible and death-promoting Bax protein. Genes Dev 1996;10:461–77.
15. Green DR, Reed JC. Mitochondria and apoptosis. Science 1998;281: 1309–12.
16. Shuler M, Bossy-Wetzel E, Goldstein JC, Fitzgerald P, Green DR. p53 induces apoptosis by caspase activation through mitochondrial cytochrome *c* release. J Biol Chem 2000;275:7337–42.
17. Thornberry NA, Lazebnik Y. Caspases: enemies within. Science 1998;281:1312–6.
18. Ryan KM, and Vousden KH. Characterization of structural p53 mutants which show selective defects in apoptosis but not cell cycle arrest. Mol Cell Biol 1998;18:3692–8.
19. Cadwell C, Zambetti GP. The effects of wild-type p53 tumor suppressor activity and mutant p53 gain-of-function on cell growth. Gene 2001;277:15–30.

20. Keshelava N, Seeger RC, Groshen S, Reynolds CP. Drug resistance patterns of human neuroblastoma cell lines derived from patients at different phases of therapy. Cancer Res 1998;58:5396–05.
21. Wallace-Brodeur RR, Lowe SW. Clinical implications of p53 mutations. Cell Mol Life Sci 1999;55:64–75.
22. Keshelava N, Zuo JJ, Waidyaratne NS, Triche TJ, Reynolds CP. p53 mutations and loss of p53 function confer multidrug resistance in neuroblastoma. Med Pediatr Oncol 2000;35:563–8.
23. Tweddle DA, Malcolm AJ, Bown N, Pearson AD, Lunec J. Evidence for the development of p53 mutations after cytotoxic therapy in a neuroblastoma cell line. Cancer Res 2001;61:8–13.
24. Diaspro A, Corosu M, Ramoino P, Robello M. Two-photon excitation imaging based on a compact scanning head. IEEE Eng Med Biol 1999;18:18–22.
25. Palù G, Palumbo M, Antonello C, Meloni GA, Marciani-Magno S. A search for potential antitumor agents: biological effects and DNA binding of a series of anthraquinone derivatives. Mol Pharmacol 1985;29:211–7.
26. Ricotti E, Fagioli F, Garelli E, Linari C, Crescenzio N, Horenstein AL, Pistamiglio P, Vai S, Berger M, Cordero di Montezemolo L, Madon E, Basso G. *c-kit* is expressed in soft tissue sarcoma of neuroectodermic origin and its ligand prevents apoptosis of neoplastic cells. Blood 1998;91:2397–405.
27. Palumbo M, Marciani-Magno S. Interaction of deoxyribonucleic acid with anthracenedione derivatives. Int J Biol Micromol 1983;5:301–7.
28. McGhee JD, Von Hippel PH. Theoretical aspects of DNA-protein interactions. Cooperative and non-cooperative binding of large ligands to a one-dimensional homogeneous lattice. J Mol Biol 1974; 86:469–89.
29. Nicoletti I, Migliorati G, Pagliacci MC, Grignani F, Riccardi C. A rapid and simple method for measuring thymocyte apoptosis by propidium iodide staining and flow cytometry. J Immunol Meth 1991;139:271–9.
30. Faulkner G, Pallavicini A, Comelli A, Salamon M, Bortoletto G, Ievolella C, Trevisan S, Kojic S, Dalla Vecchia F, Laveder P, Valle G, Lanfranchi G. FATZ, a filamin-actin, and telethonin-binding protein of the Z-disc of skeletal muscle. J Biol Chem 2000;275:41234–42.
31. Fisher RA, Yates F. Test of significance based on the normal distribution. In: Statistical tables for biological, agricultural and medical research. Edinburgh: Oliver and Boyed, 1943.
32. Sinha BK. Topoisomerase inhibitors. Drugs 1995;49:11–9.
33. Caprinico G, Binaschi M, Borgnetto ME, Zunino F, Palumbo M. A protein-mediated mechanism for the DNA sequence-specific action of topoisomerase II poisons. Trends Pharmacol Sci 1997;18:303–46.
34. Pommier Y, Schwartz RE, Zwelling LA, Kerrigan D, Mattern MR, Charcosset JY, Jacquemin-Sablon A, Kohn KW. Reduced formation of protein-associated DNA strand breaks in Chinese hamster cells resistant to topoisomerase II inhibitors. Cancer Res 1986;46:611–6.
35. Sehested M, Jensen PB. Mapping of DNA topoisomerase II poisons (etoposide, clerocidin) and catalytic inhibitors (aclarubicin, ICRF-187) to four distinct steps in the topoisomerase II catalytic cycle. Biochem Pharmacol 1996;51:879–86.
36. Karpinich NO, Tafani M, Rothman RJ, Russo MA, Farber JL. The course of etoposide-induced apoptosis from damage to DNA and p53 activation to mitochondrial release of cytochrome *c*. J Biol Chem 2002;277:16547–52.
37. Komarov PG, Komarova EA, Kondratov RV, Christov-Tselkov K, Coon JS, Chernov MV, Gudkov AV. A chemical inhibitor of p53 that protects mice from the side effects of cancer therapy. Science 1999; 285:1733–7.
38. Marchenko ND, Zaika A, Moll U. M. Death signal-induced localization of p53 protein to mitochondria. J Biol Chem 2000;275:6202–12.
39. Sansome C, Zaika A, Marchenko ND, Moll UM. Hypoxia death stimulus induces translocation of p53 protein to mitochondria. FEBS Lett 2001;488:110–5.
40. Li PF, Dietz R, von Harsdorf R. p53 regulates mitochondrial membrane potential through reactive oxygen species and induces cytochrome c-independent apoptosis blocked by Bcl-2. EMBO J 1999;18: 6027–36.
41. Gao C, Tsuchida N. Activation of caspases in p53-induced transactivation-independent apoptosis. Jpn J Cancer Res 1999;90:180–7.
42. Lee H. Protein kinase C involvement in aloe-emodin- and emodin-induced apoptosis in lung carcinoma cell. Br J Pharmacol 2001;134: 1093–103.
43. Lee H, Hsu S, Liu M, Wu C. Effects and mechanisms of aloe-emodin on cell death in human lung squamous cell carcinoma. Eur J Pharmacol 2001;431:287–95.
44. Kuo P, Lin T, Lin C. The antiproliferative activity of aloe-emodin is through p53-dependent and p21-dependent apoptotic pathway in human hepatoma cell lines. Life Sci 2002;71:1879–92.
45. Pommier Y, Fese MR, Goldwasser F. Topoisomerase II inhibitors: the epipodophyllotoxin, *m*-AMSA and the ellipticine derivatives. In: Chabner BA, Longo DL, eds. Cancer chemotherapy and biotherapy. Philadelphia: Lippincott-Raven, 1996. 435–61.
46. Mueller SO, Stopper H. Characterization of the genotoxicity of anthraquinones in mammalian cells. Biochim Biophys Acta 1999;1428: 406–14.
47. Shuler M, Green DR. Mechanisms of p53-dependent apoptosis. Biochem Soc Trans 2001;29:684–8.
48. Burns TF, El-Deiry WS. The p53 pathway and apoptosis. J Cell Physiol 1999;181:231–9.